LETTERS

Fine-tuning of pre-balanced excitation and inhibition during auditory cortical development

Yujiao J. Sun[1], Guangying K. Wu[1], Bao-hua Liu[1], Pingyang Li[1], Mu Zhou[1], Zhongju Xiao[4], Huizhong W. Tao[1,3] & Li I. Zhang[1,2]

Functional receptive fields of neurons in sensory cortices undergo progressive refinement during development[1–4]. Such refinement may be attributed to the pruning of non-optimal excitatory inputs, reshaping of the excitatory tuning profile through modifying the strengths of individual inputs, or strengthening of cortical inhibition. These models have not been directly tested because of the technical difficulties in assaying the spatiotemporal patterns of functional synaptic inputs during development. Here we apply *in vivo* whole-cell voltage-clamp recordings to the recipient layer 4 neurons in the rat primary auditory cortex (A1) to determine the developmental changes in the frequency–intensity tonal receptive fields (TRFs) of their excitatory and inhibitory inputs. Surprisingly, we observe co-tuned excitation and inhibition immediately after the onset of hearing, suggesting that a tripartite thalamocortical circuit with relatively strong feedforward inhibition is formed independently of auditory experience. The frequency ranges of tone-driven excitatory and inhibitory inputs first expand within a few days of the onset of hearing and then persist into adulthood. The latter phase is accompanied by a sharpening of the excitatory but not inhibitory frequency tuning profile, which results in relatively broader inhibitory tuning in adult A1 neurons. Thus the development of cortical synaptic TRFs after the onset of hearing is marked by a slight breakdown of previously formed excitation–inhibition balance. Our results suggest that functional refinement of cortical TRFs does not require a selective pruning of inputs, but may depend more on a fine adjustment of excitatory input strengths.

To account for the refinement of spike receptive fields (that is, receptive fields of spiking/suprathreshold responses) in sensory cortices during postnatal development, three synaptic mechanisms can be proposed (Fig. 1a). First, selective pruning of excitatory inputs at receptive field peripheries reduces the total range of inputs. Second, modifying the strengths of individual inputs, for example weakening the inputs at receptive field peripheries, can effectively reduce the size of the spike receptive field without changing the total input range. Third, broadening of the inhibitory tuning and/or strengthening of inhibition can also effectively reduce the spike receptive field size. However, these models could not be directly revealed by previous anatomical, extracellular recording or cortical slice studies. It is also worth noting that although inhibition is proposed to play an important role in regulating the critical period for cortical plasticity[5], how the inhibitory circuits undergo developmental changes has not been well elucidated. In this study, we address these issues in the rat A1, the functional development of which is marked by a progressive refinement of the tonotopic map and sharpening of spike TRFs of neurons[3,6]. Synaptic TRFs in the recipient layer 4 of the adult A1 are characterized by approximately balanced excitation and inhibition as well as a stereotypic temporal delay of inhibition relative to excitation[7–10], which can be attributed to a tripartite thalamocortical feedforward circuit[9,11,12].

To examine the developmental changes in synaptic TRFs, whole-cell voltage-clamp recordings were made from layer 4 neurons of rats at different ages. Brief tones of various frequencies and intensities were applied to map TRFs (see Methods). Excitatory responses were recorded at −80 mV and inhibitory responses at 0 mV. As shown in Fig. 1b, these synaptic inputs could be reasonably clamped. We first examined whether there was an initial mismatch between excitatory and inhibitory TRFs in early development, as suggested by a study in the developing *Xenopus* retinotectal system[13]. At postnatal day 12–13 (P12–P13), the ear canals are just opened and auditory responses can first be detected in the A1 (refs 3, 6). Surprisingly, at this stage right after the onset of hearing, excitatory and inhibitory TRFs already appeared well matched in the frequency–intensity space (Fig. 1c). The intensity thresholds for evoking excitatory and inhibitory responses were both notably high, mostly at or above 70 dB sound pressure level. Comparison of excitatory and inhibitory tuning curves (that is, the envelope of peak response amplitudes) revealed that they did not match well at the threshold intensity (Fig. 1d, 70 dB). However, at intensities above the threshold, they did match reasonably well in terms of frequency range and shape (Fig. 1d, 90 dB; Supplementary Fig. 1), like those reported in the adult A1 (refs 7–9).

To quantify the degree of mismatch between the excitatory and inhibitory tuning curves, we used a mismatch index (MMI; see Methods). For a group of P12–P14 neurons, MMI value was in general high for synaptic tuning curves at threshold intensity (Fig. 1e). This, however, should not be simply interpreted as poorly matched excitatory and inhibitory tunings; rather, it can be attributed to the unreliability of synaptic responses at the threshold and the limited number of sampling trials. In fact, similarly high MMI values at threshold intensity were also observed for adult neurons (Fig. 1e). This argues for the necessity of examining excitation–inhibition balance at intensity levels above threshold. Indeed, at higher intensities, P12–P13 neurons exhibited low MMI values comparable to adult neurons (Fig. 1e), indicating that the excitation–inhibition balance as observed in the adult A1 is already established at stages right after the onset of hearing. Given that the intensity threshold for the auditory brainstem response (ABR) at P12–P13 is similarly high as the cortical response (70–100 dB)[14,15], the cortex and subcortical nuclei may not be effectively driven under usual auditory environments at stages around the onset of hearing. Therefore the establishment of excitation–inhibition balance is likely independent of auditory experience, reminiscent of the formation of ocular dominance columns and orientation maps in the

[1]Zilkha Neurogenetic Institute, Keck School of Medicine, University of Southern California, Los Angeles, California 90089, USA. [2]Department of Biophysics and Physiology, Keck School of Medicine, University of Southern California, Los Angeles, California 90089, USA. [3]Department of Cell and Neurobiology, Keck School of Medicine, University of Southern California, Los Angeles, California 90089, USA. [4]Department of Physiology, School of Basic Medical Sciences, Southern Medical University, Guangzhou 510515, China.

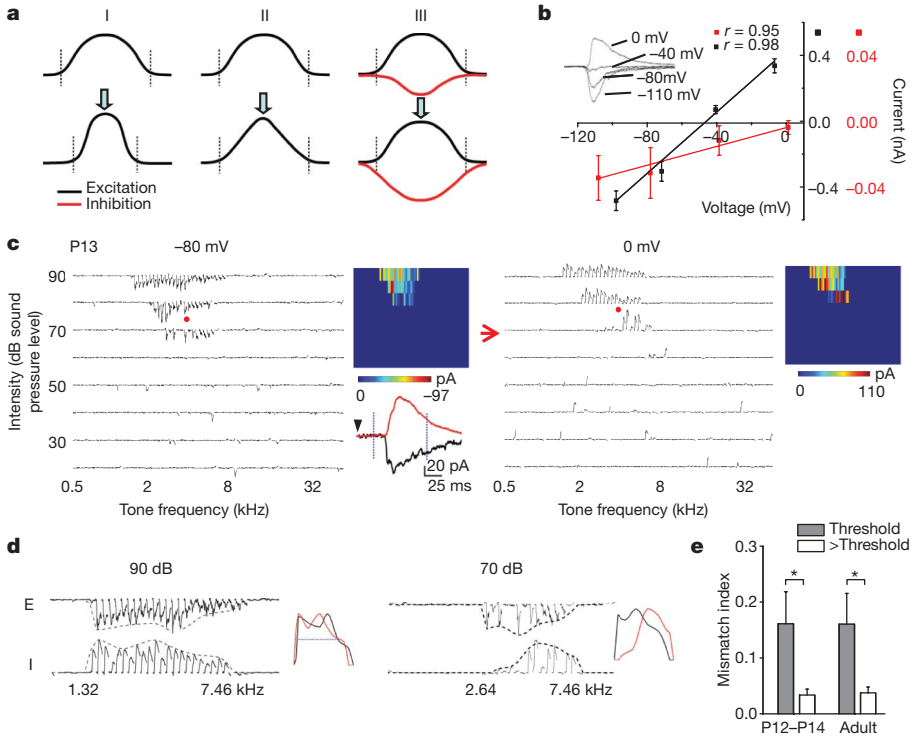

Figure 1 | The synaptic TRFs shortly after the onset of hearing. **a**, Three synaptic models for the functional refinement of sensory spike receptive fields (reduction in the size of receptive fields). Curves represent tuning profiles of excitation (black) and inhibition (red) along a sensory space. A pair of dotted vertical lines indicate the total response range of excitatory inputs. I, pruning of peripheral excitatory inputs (that is, reduced total response range). II, adjustment of input strengths without pruning of inputs. III, broadening and strengthening of cortical inhibition. **b**, Current–voltage curves for a recorded A1 neuron. Inset, average traces of synaptic currents (five repeats) of the neuron evoked by a noise stimulus. Average amplitude was measured within the 1–2 ms (red) and 21–22 ms (black) windows after the onset of the average synaptic response recorded at −80 mV. Correlation coefficient (r) is shown. **c**, TRFs of excitatory and inhibitory inputs for an example P13 neuron. Arrays of traces depict the excitatory (−80 mV) and inhibitory (0 mV) currents evoked by individual tone stimuli at various frequencies and intensities. Red arrow marks the intensity threshold. Colour map depicts the peak amplitudes of tone-evoked synaptic currents within the TRF. The example excitatory (black) and inhibitory (red) responses evoked by the same tone (indicated by red dots) were enlarged. Dotted vertical lines mark the 75-ms window for plotting individual small traces in the array. **d**, Frequency tuning curves of excitatory (E) and inhibitory (I) inputs to the same cell as in **b** at two intensities: the threshold (70 dB) and 20 dB above the threshold (90 dB). The starting and ending frequencies for the inhibitory tuning were marked. Right, the tuning curves are normalized and superimposed (E, black, reversed in polarity). Blue line indicates the half-peak level. **e**, Mismatch indices at threshold intensity (grey) and an intensity of 20 dB above threshold (white). For two P12–P14 cells exhibiting an intensity threshold of 80 dB sound pressure level, MMI was derived at 10 dB above the threshold. $*P < 0.005$, paired t-test ($n = 8$, 6 for P12–14 and adult, respectively). Error bar, s.d.

developing visual cortex, which is independent of visual experience[16,17]. These observations also support the previous hypothesis that at or even before the onset of hearing, the hard wiring is already present between auditory nuclei in the ascending pathway[18].

We next examined older stages. Compared with P12–P13, the intensity threshold for synaptic responses at P16 drastically reduced and the frequency–intensity area for synaptic responses markedly expanded (Fig. 2a). The intensity threshold did not appear to decrease further after P16 (Fig. 2b, c). For all the neurons, excitatory and inhibitory synaptic TRFs appeared largely matched (Fig. 2a–c). Comparing the synaptic tuning curves at the same relative intensity level (Fig. 2d), we did not observe appreciable developmental changes in the total frequency response range (TFRR) of synaptic inputs (see Methods). However, the shape of the excitatory tuning curve in relation to that of the inhibitory tuning curve appeared quite different between P16 and P80. At P16, the excitatory and inhibitory tuning curves both exhibited a broad peak, and they matched exquisitely. At P80, the peak of the excitatory tuning curve appeared much sharpened, whereas that of the inhibitory tuning curve remained broad (Fig. 2d and Supplementary Fig. 1). Thus the excitatory and inhibitory tuning curves at P80 appeared less matched. This observation of a slight mismatch between excitatory and inhibitory tunings is consistent with our previous report[10], which shows that a relatively broader inhibitory tuning can generate an equivalent lateral inhibitory sharpening effect.

To summarize the developmental changes in synaptic TRFs, neurons were grouped into four developmental stages: stage 1 (ST1), from P12 to P14; ST2, from P15 to P18; ST3, from P19 to P25; and ST4, P80 and older. There was a rapid decrease in intensity threshold from ST1 to ST2 both for excitatory and inhibitory TRFs (Fig. 3a). The intensity threshold of the inhibitory TRF was mostly the same as that of the excitatory TRF. It was slightly ($\leq$10 dB) higher in only a small fraction of neurons. In parallel, the intensity threshold of spike TRFs, as examined by cell-attached recordings (see Methods), became lowered with development (Fig. 3a), which is consistent with previous results[3,6]. This change in intensity threshold is likely attributed to the functional maturation of the periphery, because the intensity threshold for ABR decreases from 70 to 100 dB at P12–P13 to 30–50 dB at P16 (refs 14, 15). The ranges of excitatory and inhibitory inputs became enlarged from ST1 to ST2, as shown by the TFRRs at 10 dB above threshold (Fig. 3b). The TFRRs did not change further after ST2 (Fig. 3b). The bandwidth of the excitatory tuning curve at the level of 50% of the peak (BW50%) initially increased from ST1 to ST2 (Fig. 3c), consistent with the change in TFRR. However, after ST2, it significantly decreased, indicating that the shape of the excitatory tuning curve is sharpened without reducing the total range of inputs. In contrast, the half-peak bandwidth of the inhibitory tuning curve remained stable after ST2 (Fig. 3c), indicating that the inhibitory tuning does not undergo a significant developmental sharpening. The differential development of excitatory and inhibitory tunings leads to a slight breakdown of

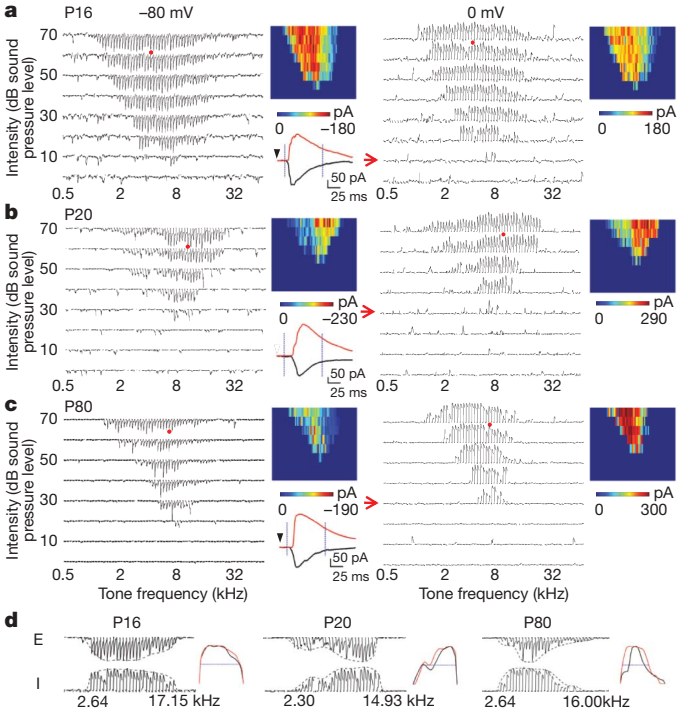

Figure 2 | Synaptic TRFs at later developmental stages. **a**–**c**, Synaptic TRFs of example neurons at P16 (**a**), P20 (**b**) and P80 (**c**), respectively. **d**, Frequency tuning curves of excitatory and inhibitory inputs at the intensity of 20 dB above threshold for cells shown in **a**–**c**. Presentation is the same as in Fig. 1.

the previously formed excitation–inhibition balance, as indicated by a significantly higher MMI at ST4 than at ST2 (Fig. 3d). At more mature stages, a relatively broader inhibitory tuning was observed for neurons exhibiting various characteristic frequencies (Supplementary Fig. 2). It is worth noting that despite the slight mismatch, excitation and inhibition are largely in balance, as indicated by the strong correlation between their amplitudes (Supplementary Fig. 3).

We note that Dorrn *et al.*[19] found the developmental establishment of balanced excitation and inhibition in the auditory cortex was a protracted process, with a relatively low level of co-tuning shortly after the onset of hearing. This apparently opposite observation may be attributed to several differences in their experimental designs. First, although our study focused on the thalamocortical circuit in layer 4, their recorded neurons spanned layers 3–6 and exhibited surprisingly broad frequency ranges of synaptic inputs cross all stages, apparently exceeding their 0.5–32 kHz testing range. Second, they chose a fixed intensity (70 dB) for examining the co-tuning of excitation and inhibition. The synaptic tuning/co-tuning may vary with the intensity level relative to the threshold of synaptic TRFs, which decreases during development. Nevertheless, both studies demonstrate that shortly after the onset of hearing, excitation and inhibition with similar amplitudes and temporal relationship to adults have already engaged in auditory-evoked responses.

We did not observe significant developmental changes in the ratio between the peak amplitudes of inhibition and excitation (*I*/*E* ratio) evoked by tones of preferred frequency, or in their absolute amplitudes (Fig. 3e). The onset latencies of excitatory and inhibitory responses become shorter with age, whereas the relative delay of inhibition to the onset of excitation (about 2 ms) remains more or less constant across different stages (Fig. 3f), further suggesting that the tripartite thalamocortical feedforward circuit is already formed at the onset of hearing.

The above data suggest that instead of a selective pruning of inputs at receptive field peripheries, adjusting the strengths and tuning pattern of excitatory inputs may be a major mechanism for the functional refinement of cortical TRFs. To understand further the impacts of the observed synaptic changes on spike receptive fields, we derived spike TRFs of the recorded neurons by integrating the experimentally determined excitatory and inhibitory synaptic conductances in an integrate-and-fire model (see Methods). To estimate

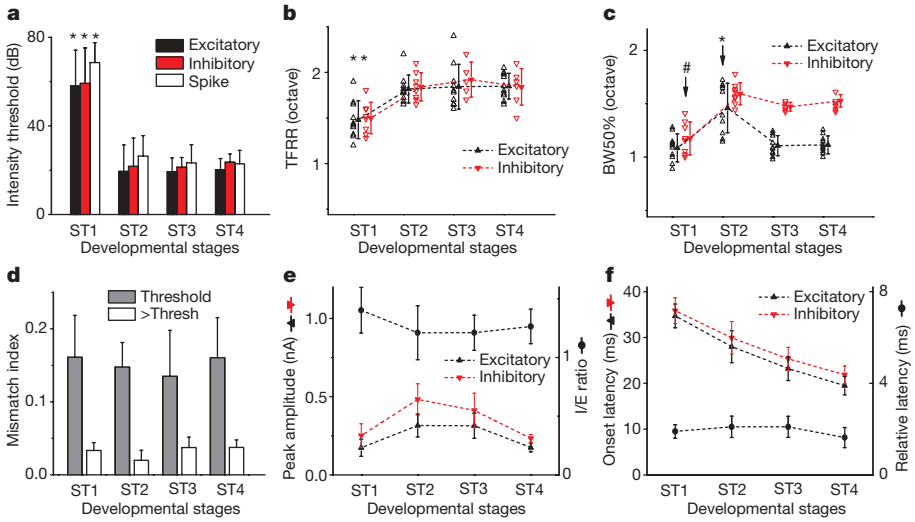

Figure 3 | Developmental changes in spectral and temporal patterns of excitatory and inhibitory inputs. **a**, Average intensity threshold of excitatory, inhibitory and spike TRFs. *Significantly higher ($P < 0.001$), ANOVA with post-hoc test ($n = 10, 10, 10, 10$ for excitatory TRFs; $n = 8, 8, 5, 6$ for inhibitory TRFs; and $n = 7, 11, 6, 14$ for spike TRFs examined by cell-attached recordings). **b**, TFRR of excitatory and inhibitory inputs at 10 dB above intensity threshold. Data were from the same recordings as in **a**. Solid symbols are average values and are connected with dashed lines for easier comparisons between neighbouring groups (the same for **c**, **e** and **f**). *Significantly lower ($P < 0.05$), ANOVA with post-hoc test. **c**, Half-peak bandwidths (BW50%) of the tuning curves in **b**. *Different in excitation; #different in inhibition; $P < 0.001$, ANOVA with post-hoc test. **d**, Mismatch indices at threshold intensity (grey) and 20 dB above threshold (white) at different stages ($n = 8, 8, 5, 6$). For 20 dB above threshold, ST2 is significantly lower than ST3 and ST4 ($P < 0.05$, ANOVA with post-hoc test). For each stage, MMI at threshold is significantly higher than at 20 dB above threshold ($P < 0.005$, paired *t*-test). **e**, Average peak amplitudes of evoked inhibitory and excitatory currents from the same recordings as in **a**. The peak amplitude was determined by averaging five responses around the best frequency at the highest intensity tested. The *I*/*E* ratio was first calculated for individual cells with both excitatory and inhibitory TRFs recorded, and then averaged (circle, $n = 8, 8, 5, 6$, respectively). **f**, Onset latencies of synaptic responses, and the relative delay of inhibition. All error bars, s.d.

the accuracy of our method of deriving spike TRFs, we performed sequential cell-attached recording and whole-cell voltage-clamp recording to obtain the bona fide spike TRF and synaptic conductances from the same cell. As shown in one example (Fig. 4a), the spike TRF derived from the synaptic conductances was largely consistent with the recorded spike TRF. For five experiments, the percentage deviation of the bandwidth of the derived spike TRF at 10 dB above threshold from that of the recorded spike TRF was 3.7% ± 10.0% (mean ± s.d.), suggesting that in these recorded cells the integration of synaptic inputs based on their spectrotemporal interactions could provide a reasonable estimation of the spike output. The summary of bandwidths of the derived spike TRFs shows that spike TRFs are first broadened from ST1 to ST2, then refined afterwards (Fig. 4b). Furthermore, spike TRFs as examined by cell-attached recordings displayed the same developmental trend (Fig. 4b). These results are consistent with previous extracellular recording studies[3,6,20], indicating that the observed changes in the patterns of excitatory and inhibitory inputs can largely explain the developmental refinement of spike TRFs.

The developmental changes in the frequency response ranges and tuning profiles suggest two phases of auditory cortical development: an initial expansion of the synaptic TRFs and a later modification of the synaptic tuning profiles. The refinement of auditory spike TRFs is mainly contributed by two factors (Fig. 4c). First, instead of the generally proposed reduction of the input range, modulation of the strengths of existing excitatory inputs leads to a sharpening of the excitatory tuning profile. Second, the relatively stable inhibitory tuning compared with the excitatory tuning results in a slight breakdown of the previous excitation–inhibition balance, allowing a lateral inhibitory sharpening effect on the spike TRF at more mature stages[10]. Thus the modulation of excitatory connections primarily guides the functional development of the auditory cortex, resulting in sharply tuned frequency selectivity and a more distinctive frequency gradient in the tonotopic map.

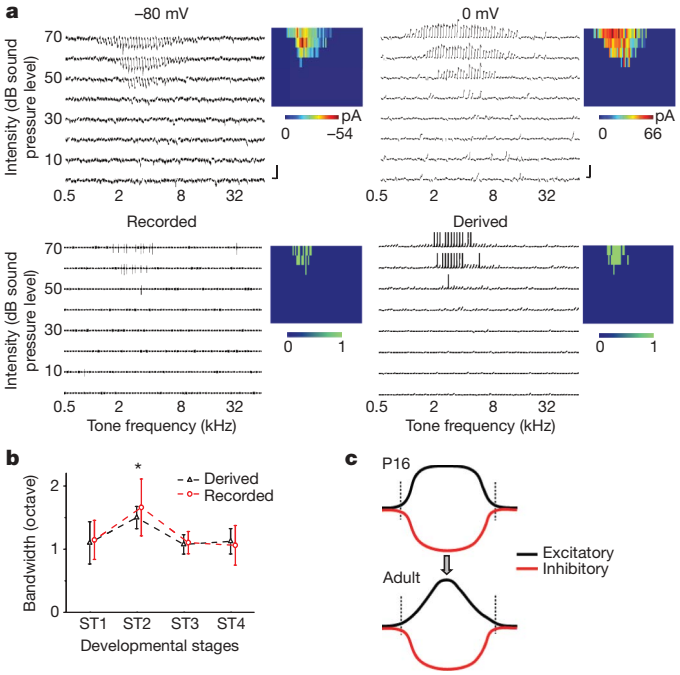

Figure 4 | Synaptic mechanisms underlying the developmental refinement of spike TRFs in A1. **a**, An example cell with cell-attached recording followed by whole-cell recording. Top panels, the excitatory (−80 mV) and inhibitory (0 mV) TRFs of the cell. Scale, 50 pA and 100 ms. Bottom left, the recorded spike TRF. Bottom right, the TRF of derived membrane potential and spike responses. Colour maps represent the peak amplitudes of synaptic inputs (top) and number of spikes evoked (bottom). **b**, Bandwidths of spike TRFs derived and recorded from cells at different stages. Bandwidth was measured at 10 dB above threshold. The value at ST2 is significantly higher ($P = 0.1$, 0.024, 0.014 between pairs of ST2–ST1, ST2–ST3 and ST2–ST4, respectively, for recorded TRFs ($n = 7, 11, 6, 14$); $P = 0.004, 0.016, 0.015$ for derived TRFs ($n = 8, 8, 5, 6$); ANOVA with post-hoc test). Error bars, s.d. **c**, A developmental model. The excitatory tuning profile is developmentally sharpened whereas the inhibitory tuning remains relatively stable. Vertical lines mark the total range of inputs.

METHODS SUMMARY

All experimental procedures used in this study were approved by the University of Southern California Institutional Animal Care and Use Committee. Sprague-Dawley rats from P12 to 3 months old were anaesthetized with ketamine and xylazine. Extracellular multiunit recordings were used to locate the rat A1 (refs 7, 9, 10). *In vivo* whole-cell voltage-clamp recordings were applied as previously described[7–10,21–24]. Excitatory and inhibitory synaptic currents were separated by clamping the cell's membrane potential at −80 mV and 0 mV, respectively. The pipette (4–7 MΩ) contained intracellular solution as follows (in mM): 125 Cs-gluconate, 5 TEA-Cl, 2 CsCl, 1 EGTA, 10 HEPES, 4 MgATP, 0.3 GTP, 10 phosphocreatine, 1.5 QX-314, pH 7.2. Cell-attached loose-patch recordings[9,10,24–26] (with pipette containing artificial cerebrospinal fluid) were used to detect spike responses of the recorded neuron. The study focused on excitatory pyramidal neurons in recipient layer 4 (refs 27, 28). Pure tones (0.5–64 kHz at 0.1 octave intervals, 25-ms duration, 3-ms ramp, a total of 568 testing stimuli) at eight sound intensities (from 0 to 70 dB sound pressure level, except for P12–P14 rats for which 20–90 dB were applied) were delivered through a calibrated free-field speaker. Frequency–intensity receptive fields (TRFs) of tone-evoked synaptic and spike responses were reconstructed, and frequency tuning curves of excitatory and inhibitory responses were derived for each testing intensity. As previously described, we computed the excitatory and inhibitory conductances[7–10,23,24,26,29,30] as well as the derived membrane potential response[8,23,24,26,31] for the recorded neurons.

Full Methods and any associated references are available in the online version of the paper at www.nature.com/nature.

Received 4 November 2009; accepted 13 April 2010.

1. Katz, L. C. & Shatz, C. J. Synaptic activity and the construction of cortical circuits. *Science* **274,** 1133–1138 (1996).
2. Fagiolini, M., Pizzorusso, T., Berardi, N., Domenici, L. & Maffei, L. Functional postnatal development of the rat primary visual cortex and the role of visual experience: dark rearing and monocular deprivation. *Vision Res.* **34,** 709–720 (1994).
3. Zhang, L. I., Bao, S. & Merzenich, M. M. Persistent and specific influences of early acoustic environments on primary auditory cortex. *Nature Neurosci.* **4,** 1123–1130 (2001).
4. Inan, M. & Crair, M. C. Development of cortical maps: perspectives from the barrel cortex. *Neuroscientist* **13,** 49–61 (2007).
5. Hensch, T. K. Critical period plasticity in local cortical circuits. *Nature Rev. Neurosci.* **6,** 877–888 (2005).
6. Chang, E. F. & Merzenich, M. M. Environmental noise retards auditory cortical development. *Science* **300,** 498–502 (2003).
7. Zhang, L. I., Tan, A. Y., Schreiner, C. E. & Merzenich, M. M. Topography and synaptic shaping of direction selectivity in primary auditory cortex. *Nature* **424,** 201–205 (2003).
8. Wehr, M. & Zador, A. M. Balanced inhibition underlies tuning and sharpens spike timing in auditory cortex. *Nature* **426,** 442–446 (2003).
9. Tan, A. Y., Zhang, L. I., Merzenich, M. M. & Schreiner, C. E. Tone-evoked excitatory and inhibitory synaptic conductances of primary auditory cortex neurons. *J. Neurophysiol.* **92,** 630–643 (2004).
10. Wu, G. K., Arbuckle, R., Liu, B. H., Tao, H. W. & Zhang, L. I. Lateral sharpening of cortical frequency tuning by approximately balanced inhibition. *Neuron* **58,** 132–143 (2008).
11. Douglas, R. J. & Martin, K. A. A functional microcircuit for cat visual cortex. *J. Physiol.* **440,** 735–769 (1991).
12. Oswald, A. M., Schiff, M. L. & Reyes, A. D. Synaptic mechanisms underlying auditory processing. *Curr. Opin. Neurobiol.* **16,** 371–376 (2006).
13. Tao, H. W. & Poo, M. M. Activity-dependent matching of excitatory and inhibitory inputs during refinement of visual receptive fields. *Neuron* **45,** 829–836 (2005).
14. Blatchley, B. J., Cooper, W. A. & Coleman, J. R. Development of auditory brainstem response to tone pip stimuli in the rat. *Brain Res.* **429,** 75–84 (1987).
15. Geal-Dor, M., Freeman, S., Li, G. & Sohmer, H. Development of hearing in neonatal rats: air and bone conducted ABR thresholds. *Hear. Res.* **69,** 236–242 (1993).
16. Chapman, B., Stryker, M. P. & Bonhoeffer, T. Development of orientation preference maps in ferret primary visual cortex. *J. Neurosci.* **16,** 6443–6453 (1996).
17. Katz, L. C. & Crowley, J. C. Development of cortical circuits: lessons from ocular dominance columns. *Nature Rev. Neurosci.* **3,** 34–42 (2002).

18. Romand, R. Modification of tonotopic representation in the auditory system during development. *Prog. Neurobiol.* **51,** 1–17 (1997).
19. Dorrn, A. L., Yuan, K., Barker, A. J., Schreiner, C. E. & Fromke, R. C. Developmental sensory experience balances cortical excitation and inhibition. *Nature* doi:10.1038/nature09119 (this issue).
20. de Villers-Sidani, E., Chang, E. F., Bao, S. & Merzenich, M. M. Critical period window for spectral tuning defined in the primary auditory cortex (A1) in the rat. *J. Neurosci.* **27,** 180–189 (2007).
21. Moore, C. I. & Nelson, S. B. Spatio-temporal subthreshold receptive fields in the vibrissa representation of rat primary somatosensory cortex. *J. Neurophysiol.* **80,** 2882–2892 (1998).
22. Margrie, T. W., Brecht, M. & Sakmann, B. *In vivo*, low-resistance, whole-cell recordings from neurons in the anaesthetized and awake mammalian brain. *Pflügers Arch.* **444,** 491–498 (2002).
23. Liu, B. H., Wu, G. K., Arbuckle, R., Tao, H. W. & Zhang, L. I. Defining cortical frequency tuning with recurrent excitatory circuitry. *Nature Neurosci.* **10,** 1594–1600 (2007).
24. Zhou, Y. *et al.* Preceding inhibition silences layer 6 neurons in auditory cortex. *Neuron* **65,** 706–717 (2010).
25. Liu, B. H. *et al.* Visual receptive field structure of cortical inhibitory neurons revealed by two-photon imaging guided recording. *J. Neurosci.* **29,** 10520–10532 (2009).
26. Liu, B. H. *et al.* Intervening inhibition underlies simple-cell receptive field structure in visual cortex. *Nature Neurosci.* **13,** 89–96 (2010).
27. Smith, P. H. & Populin, L. C. Fundamental differences between the thalamocortical recipient layers of the cat auditory and visual cortices. *J. Comp. Neurol.* **436,** 508–519 (2001).
28. Richardson, R. J., Blundon, J. A., Bayazitov, I. T. & Zakharenko, S. S. Connectivity patterns revealed by mapping of active inputs on dendrites of thalamorecipient neurons in the auditory cortex. *J. Neurosci.* **29,** 6406–6417 (2009).
29. Borg-Graham, L. J., Monier, C. & Frégnac, Y. Visual input evokes transient and strong shunting inhibition in visual cortical neurons. *Nature* **393,** 369–373 (1998).
30. Anderson, J. S., Carandini, M. & Ferster, D. Orientation tuning of input conductance, excitation, and inhibition in cat primary visual cortex. *J. Neurophysiol.* **84,** 909–926 (2000).
31. Somers, D. C., Nelson, S. B. & Sur, M. An emergent model of orientation selectivity in cat visual cortical simple cells. *J. Neurosci.* **15,** 5448–5465 (1995).

Supplementary Information is linked to the online version of the paper at www.nature.com/nature.

Acknowledgements We thank J. R. Chan for suggestions. This work was supported by grants to L.I.Z. from the US National Institutes of Health/National Institute on Deafness and Other Communication Disorders (R01DC008983, R21DC008588), the Searle Scholar Program, the Klingenstein Foundation and the David and Lucile Packard Foundation (Packard Fellowships for Science and Engineering). H.W.T. is supported by the US National Institutes of Health (EY018718 and EY019049) and the Karl Kirchgessner Foundation. Z.X. is supported by the National Natural Science Foundation of China (grant numbers 30730039, 30970982 and 30670665).

Author Contributions Y.J.S., G.K.W., P.L. and M.Z. performed the experiments. Y.J.S. and B.-h.L. analysed the data. Z.X., H.W.T. and L.I.Z. designed the experiments and analysis. H.W.T. and L.I.Z. wrote the manuscript.

Author Information Reprints and permissions information is available at www.nature.com/reprints. The authors declare no competing financial interests. Readers are welcome to comment on the online version of this article at www.nature.com/nature. Correspondence and requests for materials should be addressed to L.I.Z. (liizhang@usc.edu) or H.W.T. (htao@usc.edu).

METHODS

Animal preparation. All experimental procedures used in this study were approved under the Animal Care and Use Committee at the University of Southern California. Experiments were performed in a sound-proof booth (Acoustic Systems) as described before[7,9,10]. Sprague-Dawley rats from P12 to 3 months old were used in this study. The animals were anaesthetized intraperitoneally with ketamine and xylazine (ketamine: 45 mg kg^{-1}; xylazine: 6.4 mg kg^{-1}). Craniotomy and durotomy were performed to expose the cortex. Extracellular recordings were made with Parylene-coated tungsten microelectrodes (2 MΩ, FHC) at 500–600 μm below the pia to locate the primary auditory cortex as previously described[3,6,7]. The cortical surface was covered with pre-warmed artificial cerebrospinal fluid (in mM: NaCl 124, NaH_2PO4 1.2, KCl 2.5, $NaHCO_3$ 25, glucose 20, $CaCl_2$ 2, $MgCl_2$ 1). Frequency–intensity receptive fields of tone-evoked responses were obtained with pure-tone testing stimuli (0.5–64 kHz at 0.1-octave intervals, 25-ms duration, 3-ms ramp, a total of 568 testing stimuli) at eight sound intensities (from 0 to 70 dB sound pressure level, except for P12–P14 rats for which 20–90 dB were applied) delivered through a calibrated free-field speaker.

***In vivo* whole-cell voltage-clamp recording and loose-patch/cell-attached recording.** After mapping of A1, whole-cell recordings[7–10,21,22] were obtained from neurons located at about 450–650 μm below the pia, corresponding to the input layer of the auditory cortex[3,7,9]. This was further confirmed in several experiments with histology. We used agar (4%) to minimize cortical pulsation. For voltage-clamp recordings, the pipette (4–7 MΩ) contained intracellular solution containing the following (in mM): 125 Cs-gluconate, 5 TEA-Cl, 2 CsCl, 1 EGTA, 10 HEPES, 4 MgATP, 0.3 GTP, 10 phosphocreatine, 1.5 QX-314, pH 7.2. Recordings were made with an Axopatch 200B amplifier (Molecular Devices). The whole-cell and pipette capacitances (30–50 pF) were completely compensated and the initial series resistance (20–50 MΩ) was compensated for 50–60% to achieve an effective series resistance of 10–25 MΩ. Signals were filtered at 5 kHz and sampled at 10 kHz. Only neurons with initial resting membrane potentials more negative than −50 mV and with stable series resistance (with less than 20% change during the course of the experiment) were used for further analysis. About 50% of whole-cell recordings could be maintained in good quality to complete at least one round of the experimental test. To obtain tone-evoked synaptic conductances, neurons were clamped at −80 mV and then 0 mV (after correction of the junction potential), which are around the reversal potentials for inhibitory and excitatory currents, respectively. TRF mapping was repeated two or three times for each potential. The whole-cell recording under our experimental condition (with relatively large pipette tip-openings) targeted exclusively pyramidal neurons[7–10,21,22], which was also consistent with the observations that most layer 4 excitatory neurons are pyramidal in the auditory cortex[27,28]. The tone-evoked synaptic inputs were considered to be reasonably clamped[8–10,23], based on the linearity of the current–voltage curves, as well as the closeness of the reversible potential for the earliest component of tone-evoked currents to that of excitatory currents (0 mV; Fig. 1b). Loose-patch cell-attached recording was performed as described previously[9,10,24–26]. Glass electrodes with the same opening size containing artificial cerebrospinal fluid were used. The pipette capacitance was completely compensated. A 100–250 MΩ seal was formed on the patched neuron. The spike signal was filtered at 10 kHz and sampled at 20 kHz. Recording of spike TRFs was repeated five to ten times for each cell, and the spike number evoked by the same tone stimulus was averaged. All of the neurons recorded under this condition showed regular-spike property, consistent with sampling bias towards excitatory neurons.

Data analysis. Tone-evoked synaptic responses were identified according to their onset latencies and peak amplitudes. The onset latencies were identified during the rising phase of the response trace at the time point where the current amplitude exceeded two standard deviations of baseline fluctuation. Only responses with latencies within 15–50 ms (for young adults; 20–70 ms for early developmental stages) from the onset of tone stimulus, and with peak amplitude larger than three standard deviations of baseline fluctuation, were considered. The tone-evoked synaptic responses were normally clustered and continuously distributed within the synaptic TRF (Figs 1 and 2). The suspected spontaneous responses, especially those at peripheries of the TRFs, were further identified according to the inconsistency of their appearance or of onset latencies between trials, or the drastic change of onset latency from neighbouring frequencies (that is, ±0.1 octave if available, at the same intensity). Because the base-level activity in the auditory cortex was relatively low, the spontaneous synaptic currents were normally clearly distinguishable.

The TFRR at each testing intensity (above the threshold) was determined based on the continuity of the putative evoked synaptic responses in the frequency domain. The endings of the TFRR were determined by the appearance of two consecutive breaks of evoked responses. It should be noted that above the intensity threshold synaptic responses could be reliably elicited, although the amplitude varied between trials. At the intensity threshold, the TFRR was the frequency range covering all the evoked responses. To derive the bandwidth of the frequency tuning curve at the level of 50% of the maximum, the peak amplitudes of synaptic inputs within the TFRR were fitted with an envelope curve by using MATLAB software Envelope1.1 (developed by Lei Wang, The MathWorks), which identifies the local maxima and minima in the raw data set and then generates a smooth envelope with cubic Hermite interpolation. In this study, the intensity threshold was defined by the lowest intensity level at which both excitatory and inhibitory responses could be elicited.

MMI was calculated as the mean square error between the excitatory and inhibitory tuning curves that were normalized to the maximum response amplitude:

$$\mathrm{MMI} = \frac{1}{n}\sum_{i=1}^{n}(E_i - I_i)^2$$

where E_i is the amplitude of the excitatory input evoked by an effective tone frequency, I_i is the amplitude of the corresponding inhibitory response and n is the total number of effective tone frequencies that elicit either significant excitatory or inhibitory responses.

Excitatory and inhibitory synaptic conductances were derived according to[7–10,23,24,26,29,30]:

$$I(t) = G_r\,(V(t) - E_r) + G_e(t)(V(t) - E_e) + G_i(t)(V(t) - E_i)$$

where I is the amplitude of synaptic current at any time point, G_r and E_r are the resting conductance and resting membrane potential which were derived from the baseline currents of each recording, G_e and G_i are the excitatory and inhibitory synaptic conductance, respectively, V is the holding voltage, and E_e (0 mV) and E_i (−80 mV) are the reversal potentials. In this study, a corrected clamping voltage was used, instead of the holding voltage applied (V_h). $V(t)$ is corrected as $V(t) = V_h - R_s \times I(t)$, where R_s was the effective series resistance. A 10-mV junction potential was corrected. By holding the recorded cell at two different voltages, G_e and G_i were calculated from the equation. G_e and G_i reflect the strength of pure excitatory and inhibitory synaptic inputs, respectively. The analysis indicated that recorded synaptic currents (after subtraction of baseline) can be simply used to compare excitatory and inhibitory tuning curves under our experimental conditions.

Membrane potential and spike responses were calculated from the derived excitatory and inhibitory conductances based on an integrate-and-fire model[8,23,24,25,31]:

$$V_m(t+\mathrm{d}t) = -\frac{\mathrm{d}t}{C}[G_e(t)\times(V_m(t)-E_e) + G_i(t)\times(V_m(t)-E_i) + G_r(V_m(t)-E_r)] + V_m(t)$$

where $V_m(t)$ is the membrane potential at time t, C is the whole-cell capacitance, G_r is the resting leaky conductance and E_r is the resting membrane potential (−65 to −60 mV). To simulate spike responses, 20 mV above the resting membrane potential was set as the spike threshold and a 10-ms refractory period was used. Based on the synaptic inputs, a tone stimulus only generated at most one spike. C was measured during experiments and G_r was calculated based on the equation $G_r = C \times G_m/C_m$, where G_m, the specific membrane conductance, is 2×10^{-5} S cm^{-2}, and C_m, the specific membrane capacitance, is 1×10^{-6} F cm^{-2} (refs 23, 24, 26).